Applied Surface Science 639 (2023) 158255

Contents lists available at ScienceDirect

Applied Surface Science

journal homepage: www.elsevier.com/locate/apsusc

Full Length Article

Non-contact approach to extract Schottky barrier characteristics for gas sensitive nanostructured interfaces

Kun Cao [a], Guanyi Gong [a], Xiangyang Guo [a], Yanling He [b], Francis Chi Chung Ling [b], Wanyin Ge [d], Alan Man Ching Ng [c,*], Yongxiang Li [a,*], Jerry Yu [a,c]

[a] School of Engineering, STEM College, RMIT University, 124 La Trobe St, Melbourne VIC 3000, Australia
[b] Department of Physics, The University of Hong Kong, Pokfulam Road, Hong Kong
[c] Department of Physics, Southern University of Science and Technology, Shenzhen, 518055, China
[d] School of Materials Science and Engineering, Research Center for Auxiliary Chemistry and New Materials Development, Shaanxi University of Science and Technology, Xuefu Road, Xi'an, Shaanxi, 710021, China

ARTICLE INFO

Keywords:
Schottky diode
Schottky barrier height
Nanorod
Band structure
Ultraviolet photoelectron spectroscopy
Gas sensor
Hydrogen

ABSTRACT

Formation of high precision nanorod based surface morphologies can be engineered with nanotechnology to mimic the function of sensory hairs. Gas sensitive *I-V* characteristics unique to these surfaces require initialisation under voltage bias and temperature elevation to exploit their band structures and therefore achieve optimal gas response. Prior to detection, devising effective approaches to optimise nanorod based sensors can provide access and efficient control to downsize and significantly miniaturise current gas sensors. In this work, we devised a novel non-contact analysis approach via ultraviolet photoelectron spectroscopy (UPS) to extract specific band structure parameters specifically to locate particular bias for optimal sensor initialisation. The results from five cases all indicate how fabricated nanostructured Schottky barrier heights can be evaluated from UPS data and how their *I-V* data are correlated and also validate our band structure postulations. The obtained Schottky barrier height values from simulated band structures provided an optimal biasing condition of 0.8 V for Au-ZnO nanorod hydrogen gas sensory operation at 150 °C, demonstrating experimental validity with gas-electrical measurements. Further, the gas response data show exponential dependence with gas concentration which is highly relevant for programmable trigger response controlled sensing function based applications.

1. Introduction

Formation of gas sensitive nanostructured nanorod surfaces with high aspect ratios can mimic and improve upon the current limitations of current semiconductor gas sensors. By exploiting unique gas-electrical transducing properties from these nanosensory materials, approaches to optimise the fabrication of nanostructures gas sensors presents a significant step to access miniaturisation and greater control at the nanoscale. Sensory materials primarily function by detecting the change in surface interactions via their interface characteristics, which requires favourable positions of band-structure alignment to function. Moreover, these alignments in band-structure energy to form Schottky barriers have been linked to a material's surface morphology, crystallographic structure and stoichiometric composition dependency [1]. yet locating initialisation parameters that specifically identify the optimal voltage bias and operating temperature are highly essential. Therefore, material and electrical data extracted from sensory material during the growth phase can essentially provide crucial insight to evaluate device performance prior to testing and calibration. To initialise a Schottky barrier for gas detection, often requires the elevation of the Fermi level (voltage biasing) and weakening of bandgap energy (preheating temperature) to function optimally [2]. These values vary considerably for a variety of different sensory materials and thus, their subsequent metal-contacted interface characteristics. Therefore, to validate a sensory material and estimate the suitability of its band-structure characteristics for gas sensing, a viable non-contact approach to estimate its optimum operating conditions is highly advantageous. Without the need to conduct various electrical characterisation and gas tests, extraction of voltage and temperature conditions can be beneficial to estimate heating supply and biasing circuits to assess CMOS integration and sizing requirements.

Morphological nanostructured shapes (such as nanorods, nanowires or nanotubes) formed from sensory nanomaterials have presented

* Corresponding authors.
E-mail addresses: ngamc@sustech.edu.cn (A.M.C. Ng), yongxiang.li@rmit.edu.au (Y. Li).

https://doi.org/10.1016/j.apsusc.2023.158255
Received 6 June 2023; Received in revised form 1 August 2023; Accepted 12 August 2023
Available online 13 August 2023

unique surface characteristics as their band structure and biasing dependent electronic based sensory properties exploit the advantages of high aspect and surface area to volume ratios [3]. Additionally, presence of crystallographic defects that define the surface quality between a metal to oxide interface (Schottky barrier) can augment sensory performance under different biasing conditions. For example, research findings in [4,5] and [6] found differences between single- and poly-crystalline structures which show a bias-temperature dependency for sensory operation [7] as charge is rapidly accumulated within the crystallographic boundaries (or grain boundaries) to be elevated into the conduction band for Schottky barrier modulation. As these boundaries contain oxygen vacancies, the effect of stoichiometric composition during interface formation [8,9] particularly O^-, O_2^- and O^{2-} are considered the intrinsic defects within an oxide based sensory material that dictate gas response. For ZnO, single crystals are commonly formed along the (00 *l*) axis, and the majority of oxygen vacancies are therefore heavily dependent on surface stoichiometry, thus intrinsic defects from the metal ions bonded to oxygen of the oxide, for example, 1^+ or 2^+ ions (or lone pairs), and types of bonding associated with these often contribute to temperature dependent chemisorption for gas sensitive interactions [10]. Alternatively, examples of extrinsic defects by doping have also been explored in the works of [11] and [12], and have played different roles to augment sensory performance.

The term Schottky barrier height change has been widely accepted for evaluating gas response based sensory performance [13–15]. Analysis of band structure particularly to identify the interfacial characteristics from a Schottky barrier has been widely based on linear extrapolation from the *I-V* data of the entire surface. However, since the emergence of nanostructured sensory materials with morphological surfaces that have very high aspect ratios, such as nanorods, it has been observed that charge would concentrate at the tips of their protrusions where the highest concentration of defects is located. Therefore, such geometries from the surface morphology can augment *I-V* characteristics to a degree that is not always linear, especially at low magnitudes of bias voltage to drive current levels at the microampere (μA) or even nanoampere (nA) ranges (as unique *I-V* properties can be seen under current logarithmic scale). Under low biases, the Fermi level energy lifts charge carriers into the defect levels of the band structure and facilitates thermionic field emission as the main transport mechanism across the top thin edge of the Schottky barrier. This can occur as thermally charged carriers are driven across the interface without creating a large depletion region that results in capacitive effects. Therefore, to accurately estimate the optimal operating conditions of a nanostructured Schottky barrier, under the absence of biasing (for example during growth) requires considering alternative means of non-contact analysis to scan the surface morphology and model the band structure. Locating the ideal biasing conditions to modulate a Schottky barrier height and control its barrier height is therefore of crucial importance.

A non-contact approach to analyse the band structure of a sensory material can provide an indirect alternative to characterise surfaces particularly nanostructured Schottky barriers. Although such an approach has been applied to investigate sensory nanomaterials that form nanostructured Schottky barriers, in this work, we report how sensory parameters such as a nanostructured Schottky barrier height can be indirectly extracted using a non-contact Ultraviolet Photoelectron Spectroscopy (UPS) methodology. This assists in determining optimal operating conditions, such as voltage biasing, for gas sensing. As previous works relied heavily on linear extrapolation methods to obtain change in Schottky barrier height to evaluate sensory performance from gas response, such methodology cannot always be directly applied to non-linear *I-V* data. Therefore, in this work, we show how the UPS data can be evaluated to assist linear extrapolation methodologies to extract the nanostructured Schottky barrier height at the biasing regions that form the band structure as indicated by UPS. We expect to show that UPS can supplement an accurate estimation of barrier height. This method is applied to analyse a series of ZnO Schottky barriers formed under different annealing temperatures. Validation of their highest sensory performance is performed by measuring the gas response under their obtained optimal operating condition.

2. Theory

2.1. Gas sensing based on Schottky barriers

Schottky barriers describing planar thin film based metal-oxide interfaces have been defined in semiconductor theory [16]. However, nanostructure materials that embed presence of nanoscale morphologies protruding from surfaces represent extensions to the theory, in which enhanced properties by quantum effects at the nanoscale have been reported in [17–20]. Assuming the formation of Schottky barriers from single crystal vertical nanorod oxides sensory nanostructures, intrinsic defects play a vital role for majority charge accumulation as the potential difference is located at tips of their nanorod protrusions, which effectively modulates the magnitude of the intrinsic nanostructured Schottky barrier height to drive a thermionic electric field induced current down the vertical length of the nanorod. By applying a voltage bias, the nanostructured Schottky barrier can be controlled to a state where band structure involves the alignment of energy bands under a specific bias to reflect the most favourable conditions for charge to flow under field emission (FE), thermionic field emission (TFE) or thermionic emission (TE) transport mechanisms [16]. Investigations for device physics addressing specific types of annealed Schottky barriers operating at elevated temperatures [21] and also observed abnormal electrical behaviours that can be explained with Gaussian distribution functions [22] have been reported. For sensory based Schottky barriers formed from metal contacted nanostructured materials, their unique surface morphologies can concentrate a larger distribution of charge at their protrusions providing greater sensitivity to change with gaseous interactions.

Fig. 1 shows a Schottky diode nanostructured based gas sensory device schematic and its corresponding nanostructure energy band diagrams. In particular, Fig. 1(a) shows the typical configuration of an Au contacted ZnO nanorod array based Schottky diode as a needle probe contact is typically used to interface with the metal contacted nanorods the band structure aligns according to the elevation of the Fermi level as charge is accumulated across the interface. Here, we postulate the formation of Au contacted ZnO nanorods with diameter and length of 25 nm and 1 μm, respectively with each nanorod separated by a vacant gap. Assuming this would allow each nanorod to effective function as individual entities and perform transducer function to detect gaseous change, while a micro thin probe (not to scale) provides bias across many contacted nanorods. This effectively can form an array of parallel nanocircuits to which the impedance of a nanorod array (*I-V* data) is measured under exposure of a gaseous environment to detect change. Fig. 1(b) illustrates the band structure, electronic conduction mechanism and gas sensing mechanism representing the device physics occurring in the Au-ZnO nanorods. Formation of an effective Schottky barrier in terms of energy illustrated as a classical mechanics theory is depicted under forward neutral and reverse biasing conditions. Fig. 1(c) shows a simulated band structure of a planar Au-ZnO interface as simulated by multi-dielectric energy band diagram program [23]. Simulation parameters for input and output are provided with an ideal case being presented for an Au-ZnO Schottky barrier. Input values for Au metal workfunction, ZnO bandgap and electron affinity energy into the simulation are as given in the CRC handbook for dielectric materials to form the band structure under zero bias at 25 °C. Corresponding output as simulated for the forward turn on bias V_{FB} is 1.055 V which is effectively the Schottky barrier height (in eV).

Gas sensing mechanism for a nanostructured Schottky barrier can be further described. A Schottky barrier height change is caused by the influence of additional external gas adsorbate charge as it adsorb and undergo catalytic dissociation at the surface of the transition metal,

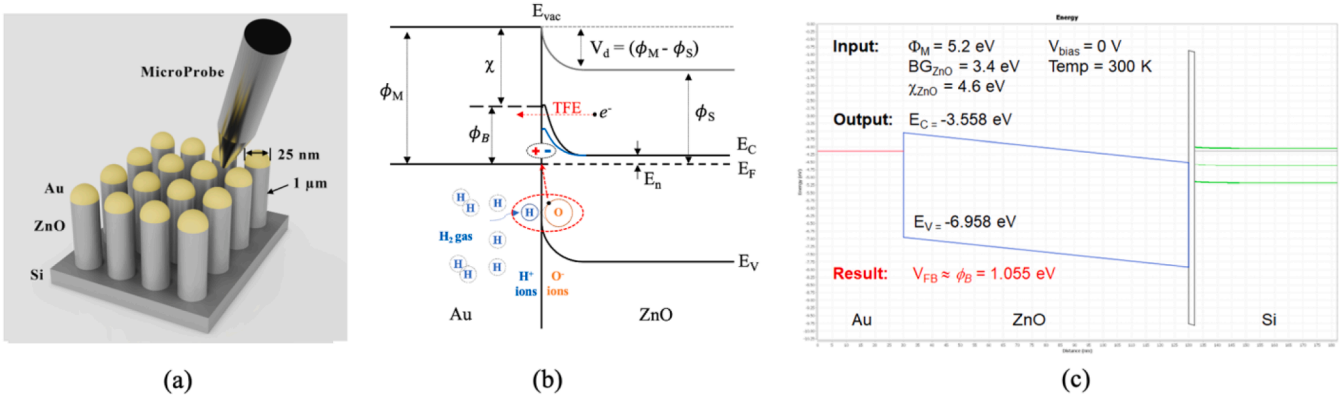

Fig. 1. (a) Schematic representation of an Au-ZnO nanorod array based Schottky diode device as analysed by electrical probe. (not drawn to scale), Au layer is deposited as a 25 nm thin layer on the tip of the nanorods. (b) Energy band diagram illustrating the band structure of Schottky barrier formed between Au and ZnO, a n-type semiconductor nanostructured material. The gas sensing mechanism shows how hydrogen gas dissociates, adsorbed and diffuses to the interface forming as a dipolar charge to cause band bending by realigning the energy bands. The main electron conduction transport mechanism focussed in this work is thermionic field emission (TFE). (c) Band structure of a planar Au-ZnO structure as simulated by multi-dielectric energy band diagram program [23] is shown as reference.

diffusing down to the metal-oxide interface. This is effectively an example of the Mott-Schottky effect that occurs without elevating the Fermi level. Instead, a charge dipolar layer at the interface is temporarily created by the gaseous adsorbates. For the case of a nanorod, the continuous presence of gas provides additional accumulation of absorbate charge along the elongated curved surface, where a "hydrogen spillover" effect occurs where the activation energy barrier is minimised resulting in the majority of dipolar charge building up at the nanorod tip interface. Here, any Schottky barrier height change induced by gas absorbate presence is reflected in the rectifying behaviour in its *I-V* characteristics and therefore stresses importance on the position of the applied bias chosen to operate the nanostructured Schottky barrier. To maximise gas response or gas sensitivity, temperature dependent biasing based on the thermionic field emission conduction mechanisms has been observed previously [24], and therefore locating their optimal operation conditions specifically the biases for ZnO and other different materials can provide functional and operational advantages.

For sensory interfaces which involve the image force charge that form the Schottky barriers and also addition of gaseous adsorbate charge and temporarily adds dipolar charge to modulate the barrier height can be described in terms of thermionic-field emission mechanism (TFE). The main use of TFE is to account for presence of surface defects as nanostructured surfaces elevate the surface area, accounting for increased presence of defects and therefore provide necessary adsorption sites for gaseous interactions. The relationship describing the current–voltage relationship can be described by the TFE equation as [16]:

$$J_{TFE} = \frac{A^{**}T\sqrt{\pi E_{00}q(\phi_{Bn} - \phi_n - V_F)}}{kcosh(E_{00}/kT)} exp\left[\frac{-q\phi_n}{kT} - \frac{q(\phi_{Bn} - \phi_n)}{E_0}\right] exp\left(\frac{qV_F}{E_0}\right) \quad (1)$$

where, E_{00} is typically described as a characteristics energy and E_0 is described the ideal energy of TFE conduction within the conduction band.

$$E_0 = E_{00}coth\left(\frac{E_{00}}{kT}\right) \quad (2)$$

as defined in [16], the maximum TFE energy at approximately at an energy E_m:

$$E_m = \frac{q(\phi_{Bn} - \phi_n - V_F)}{cosh^2(E_{00}/kT)} \quad (3)$$

To extract physical parameters from logarithmic *I-V* data using TFE theory, equation (1) can be simplified when linearity is achieved at particular voltage bias regions, as A** and image-force lowering are weak functions of the applied voltage, which assumes the exponential as the primary variable and the outlier constants neglected. When $V_F > 3kT/q$ Therefore Equation (1) can be simplified as:

$$\log J_{TFE} = \frac{-q\phi_n}{kT} - \frac{q(\phi_{Bn} - \phi_n)}{E_0} \quad (4)$$

Therefore, assuming (ϕ_n) is relatively small compared to (ϕ_{Bn}), then the first term can be essentially ignored and therefore, in terms of in terms of magnitude, the TFE barrier height energy is given as:

$$\phi_{Bn} = \frac{kT}{q} ln(J_{TFE}) \quad (5)$$

Using Equation (5), we can deduce from the logarithmic *I-V* data, under linear extrapolation estimates for the TFE barrier height energy.

As nanostructured interfaces are exposure to different gas environments, they capture temporarily, gaseous adsorbate charge and reinforces the pre-existing interface formation charge due to image force lowering. To deduce the TFE barrier height energy, linear extrapolation is applied to two sets of *I-V* data in logarithmic form and the difference in their magnitudes is determined. However, in nanostructured sensory materials, the logarithmic form of the *I-V* data may not always present linear trend and specific regions, which at specific biases may be feasibly applied. Therefore, if the optimal operating condition needs to be determined selectively, therefore, an approximate bias voltage to initialise the nanorods would need to be firstly estimated. In this work, we show that this can be achieved through modelling and optical data to find energies of the band structure and extract barrier height energy. As this energy can converge and position the voltage bias selectively, we use this result to optimise the sensory device and analyse the gas sensing performance.

2.2. Ultraviolet photoelectron spectroscopy (UPS) for nanostructured Schottky barriers

To analyse an Au-ZnO nanorod based Schottky barrier height using ultraviolet photoelectron spectroscopy (UPS) theory, analysis of the energy structure can be performed by firstly assuming metal and oxide as individual materials. Yet, the presence of nanorod surface morphologies is far from ideal as discussed above, which results in the significant accumulation of interface charge during formation. After reaching charge equilibrium, we expect a nanorod Schottky barrier height based on Au and ZnO nanorod, to significantly differ from ideal case with greater lowering from this value as band bending is highly dependent on

charge accumulation at the interface of Au-ZnO nanorod interface. Therefore, it is similarly methodical to estimate the Schottky barrier height approaching band structure estimation using UPS to analyse the ZnO nanorods under conditions with and without the presence of Au metal.

Schottky barriers describing nanostructured based metal-oxide interfaces can be defined in UPS theory as being derived from the photoelectric effect [25]. By applying the theory to describe a nanostructured Schottky barrier, the energy potential relationship can therefore be related by the difference in metal workfunction and oxide electron affinity is equated as:

$$\phi_B = \phi_M - \chi = V_d + E_n \tag{6}$$

where, ϕ_B is nanostructured Schottky barrier, ϕ_M is the work function of the metal, χ is the electron affinity, V_d is the band bending energy potential difference and E_n is energy elevated between the Fermi level and conduction band, respectively. Note that E_n is commonly considered a negligible term (in the literature), however under a biasing condition, especially as an applied voltage bias approaches the value of the Schottky barrier height electrons overcome the charge equilibrium state and align the Schottky barrier, to facilitate favourable conditions for current to therefore flow.

To equate a nanostructured Schottky barrier height energy in terms of quantum energies, the band bending energy (V_d) can also be expressed as a bipolar difference term. Thus, in a formed between a metal onto the surface of nanostructured oxide structure, the V_d potential difference can be expressed as:

$$V_d = \phi_M - \phi_S \tag{7}$$

where, ϕ_S is the work function of the ZnO, Therefore, in terms of photoelectric UPS theory, a nanostructured Schottky barrier based on a metal and semiconductor structure can be equated as:

$$\phi_B = \phi_M - \chi = \phi_M - \phi_S + E_n \tag{8}$$

To estimate the nanostructured Schottky barrier as applied to Au contacted ZnO nanorods, measured parameters for Fermi edge, VBM and cut-off energy under UPS analysis method can obtain accurate values for ϕ_M, ϕ_S, E_n energies to form the band structure model, respectively.

Fig. 2 illustrates a nanostructured Schottky barrier as extracted from the surface Au metal contacted ZnO using ultraviolet photoelectron spectroscopy. Fig. 2(a) shows the device schematic of a nanostructured Schottky diode device and under UPS analysis the surface of Au and ZnO nanorods is exposed to He laser sequentially. Fig. 2(b) shows a band structure of Au and ZnO, typically obtained by UPS analysis. This data is used in the subsequent section for the estimation of the nanostructured Schottky barrier height. Within the parameters of this work, we show our approach is simple and adequate without further data from photoemission band mapping using momentum-energy resolved or angle resolved photoemission spectroscopy (PES).

3. Experimental

To verify our theoretical postulations, Au interfaced ZnO nanorods are fabricated and analysed by UPS and *I-V* analysis. Non-contact photoelectric UPS analysis are conducted to identify band structure energy and contract probe measurements are conducted to obtain the *I-V* data.

3.1. Fabrication

In this work, five devices of metal contacted nanorod arrays are fabricated by semiconductor processing Pulse Laser Deposition (PLD) and subsequent annealing processes. *N*-type (1 0 0) Silicon (Si) wafers (University Wafers, USA) are prepared and diced into 10 × 10 mm^2 pieces using a Disco DAD123 dicing saw. The substrates are then cleaned using the standard two-step RCA cleaning methods in semiconductor processing [26] and stored in deionised (DI) pure H_2O and blow-dried with N_2 at room temperature. Ohmic contacts comprising Ti/Au (40 and 100 nm) are deposited on the backside of the substrates by e-beam deposition [27]. For the formation of the ZnO nanorods, PLD deposition (Lenton) and annealing processing are performed subsequently.

Fig. 3 shows a schematic diagram of the interior of the PLD deposition chamber (Kurt J. Lesker), and deposition is performed under steps. Deposited substrates are cleaned with ethanol, surface dried with N_2 and placed into the PLD chamber with the (ohmic contact face down), which is then vented in two steps, the first via a rotary pump (to low vacuum pressure) and then second via a cryogenic pump down to a base and working pressure of 133 mbar. Subsequent to venting, the substrates are placed onto a heating stage which rotates at 3 rpm and is heated to 300 °C by ramping at a rate of 1 °C/min prior to deposition to prevent any growth of SiO_2.

During deposition, an ArF excimer laser (Class 5) is calibrated at 193 nm and pulsed at 5 Hz with a maintained output power of 230 J/pulse onto the target. The laser beam is focused onto the target via an optical lens at a 45-degree angle onto a rotating ZnO target (J.K. Lesker) of 99.99% purity. The rotation of the target is maintained at 20 rpm which is positioned at a distance 50 mm away. Deposition thickness is calibrated to an average growth of 3 nm per min via a Quartz thickness monitor (Sigma-Aldrich) and thus, the deposition process is performed over 6 h to deposit a thickness of 1 μm. The deposited ZnO samples are then placed into an annealing tube furnace (ThermoFisher Scientific)

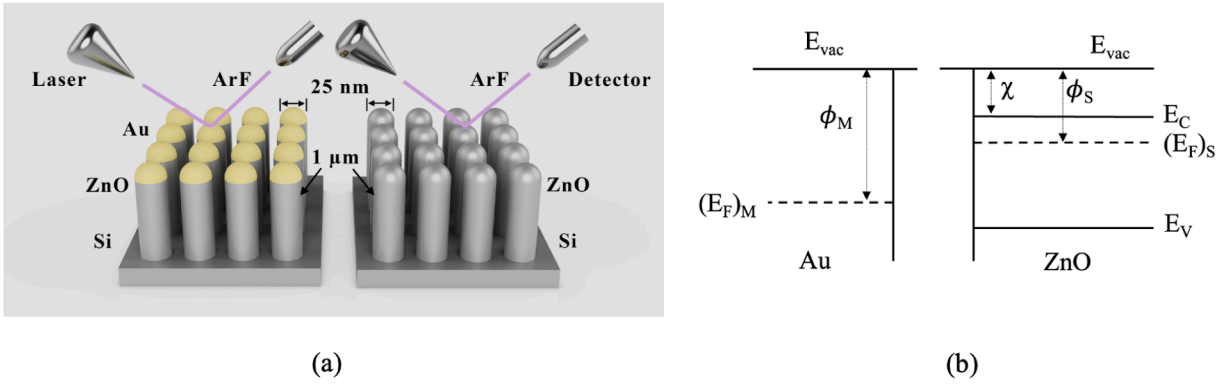

Fig. 2. (a) Schematic representation of a ZnO nanorod array based Schottky diode device with and without Au contacts as analysed by ultraviolet photoelectron spectroscopy (UPS). (b) Energy band diagrams obtained by UPS illustrating the band structure of Au and ZnO nanorods separately prior to barrier formation. The postulation is to extracted specific parameters from the band structure using UPS such as ϕ_M, E_C, E_V and E_F to directly estimate the Schottky barrier height for Au-ZnO nanorods.

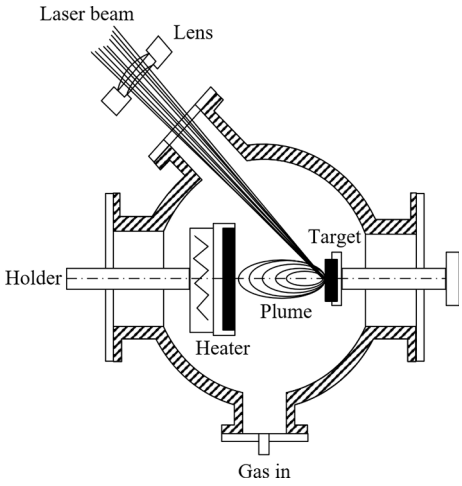

Fig. 3. Schematic diagram of the PLD chamber interior showing their components. PLD deposition process involves a high-power pulsed laser beam focused via lens into the chamber to strike a source target for plume vapour based deposition. Source material is vaporised ejecting from the target as a plasma plume, accumulating deposits onto the polished side of the *n*-type Si substrate located onto a heated stage platform.

with a gaseous environment of 20% O_2 in Ar gas, at a flow rate of 1000 sccm. Post annealing process is performed separately to fabricate five devices by ramping the annealing temperature from 25 °C to five different temperatures (300 °C, 400 °C, 500 °C, 600 °C, 700 °C) to fully oxidise the ZnO nanorods on the substrates. The annealing process is carried out by increasing temperature at a rate of 2 °C/min ramp up, until the target is reached and held for 60 min, and subsequently the temperature is ramped down at 2 °C/min until room temperature.

The nanostructured (nanorod based) Schottky contacts are formed by using a thermal evaporation system (Denton) to deposit a 25 nm thick layer of Au. The thermal evaporator chamber is vented to a pressure of 1.33×10^{-6} mbar. For contact deposition a pure Au 99.99% target (Kurt J. Lesker) is used for Au contact deposition onto the ZnO nanorod surface via stainless steel shadow mask and a standard e-beam evaporation procedure is performed using a quartz crystal microbalance thickness monitor set to 25 nm during deposition. The purpose of the Au deposition is intended to create experimentally high-quality metal-oxide Schottky contact in the form of nanorods.

3.2. Material characterisation

For material characterisation, the material's surface morphology is characterised via SEM (FEI Nova NanoSEM 200) and AFM (Veeco Instruments), while the crystallographic structure is analysed by TEM (JEOL 2100 FEGTEM), surface stoichiometry of the ZnO nanorods is characterised using an XPS (JSM-7001F, JEOL, Japan). Ultraviolet photoelectron spectra (UPS) are obtained using an ESCALAB 250xi XPS (Thermo Fisher). The helium (He) discharge lamp with energies of 21.2 eV is used to excite electrons from the valence band. Under UPS, the Au on ZnO nanorods and ZnO nanorods are measured separately for their binding energy profile for calculation of nanostructured Schottky barrier height.

The surface morphology of the as-deposited ZnO is analysed by SEM, while the post annealed ZnO nanorods are analysed by AFM methods. Fig. 4 shows the SEM of the as-deposited ZnO nanorod array, with the figure inset taken at a 45° inclination showing the cross-sectional SEM revealing a nanorod height of 1 μm. Hemispherical tips of the nanorods can be observed from the analysis. To further study the nanorod tips, AFM analysis is conducted for the post annealing conditions of the five films. Fig. 5 shows a 3D surface micrographs scan by AFM of the ZnO nanorods as post-annealed at (a) 300 °C, (b) 400 °C, (c) 500 °C, (d)

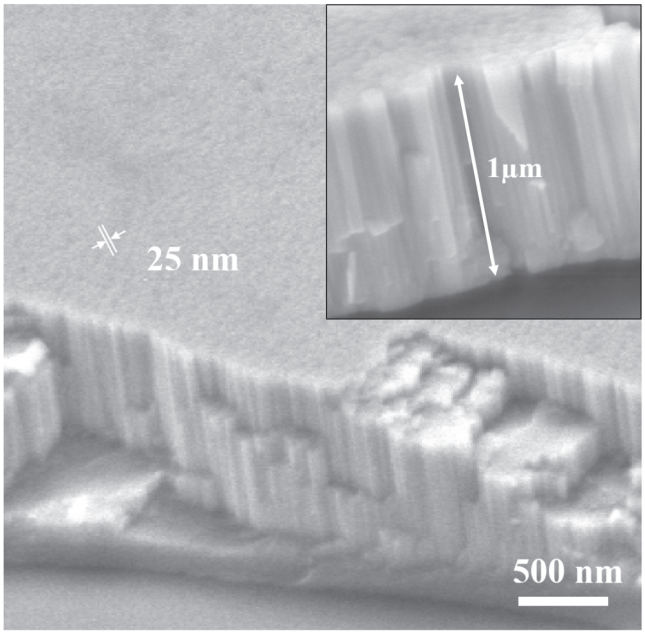

Fig. 4. SEM Micrograph (captured at an inclination of 45° to the horizontal) of the as-deposited ZnO nanorods revealing growth of an ordered array of nanorods with an average nanorod diameter of 25 nm. The inset (top left figure) shows the cross-sectional SEM captured, revealing an average height of the nanorods as 1 μm.

600 °C and (e) 700 °C, respectively. Each surface scan indicates the presence of a curved hemispherical nanorod tip diameter of approximately 25 nm, verifying minimal change in curvature and surface morphology.

Crystallographic structure analysis of the as-deposited ZnO is analysed by TEM while the post annealed ZnO nanorods are analysed by XRD methods. Fig. 6 shows HRTEM of a nanorod surface with the inset showing an individual nanorod of 25 nm diameter. Fig. 6(a) shows the interplanar spacing within the crystallographic structure of the nanorod of (0 0 2) direction with a *d*-spacing of 0.26 nm. Fig. 6(b) shows the captured SAED pattern from the TEM from Fig. 6(a), and the (0 0 1) and (1 0 0) orientation are marked in the diagram. Fig. 7 shows the XRD diffractogram as measured of the ZnO nanorods. XRD analysis of the ZnO nanorods post-annealed at the five temperatures from 300 to 700 °C revealed dominant peaks of a single crystal ZnO with directions in (0 0 2) and (0 0 4) at 2θ values of 34.3° and 72.8° corresponding to nanorod growth in the vertical *c*-axis direction, and presence of underlying *n*-type (1 0 0) Si substrate direction can also be seen in the broad peak at 2θ values at 68.2° corresponding to the (1 0 0) direction.

Stoichiometric compositional analysis is performed on the post-annealed ZnO nanorods at the five temperatures from 300 to 700 °C using XPS methods. Fig. 8 shows the XPS spectrograph, with Fig. 8(a) & 8(b) illustrating the binding energy data in the O1s and Zn2p region, respectively. The data in Fig. 8(a) shows the binding energy peaks for O1s, indicating the presence of Zn-O and O^{x-} defect bonds as modelled by two subpeaks fitted using Gaussian distribution at 529.7 eV and 531.4 eV, respectively. Results show a level of shouldering in the fitting of the data which can be attributed to O^{x-} peaks surface defects, which indicates a gradual increase in surface defect presence from the c-axis growth of long stable ZnO nanorods when annealed with increasing annealing temperature. As ZnO possesses a single crystal form, such an increase in surface defects due to increasing annealing temperature can therefore result in slightly different band structures when formed. This is in contrast to the observed data from ZnO nanograins [28], which observed a maximum in defect presence as annealed at 500 °C. The data in Fig. 8(b) shows the Zn binding energy peaks which for both 2p1/2 and

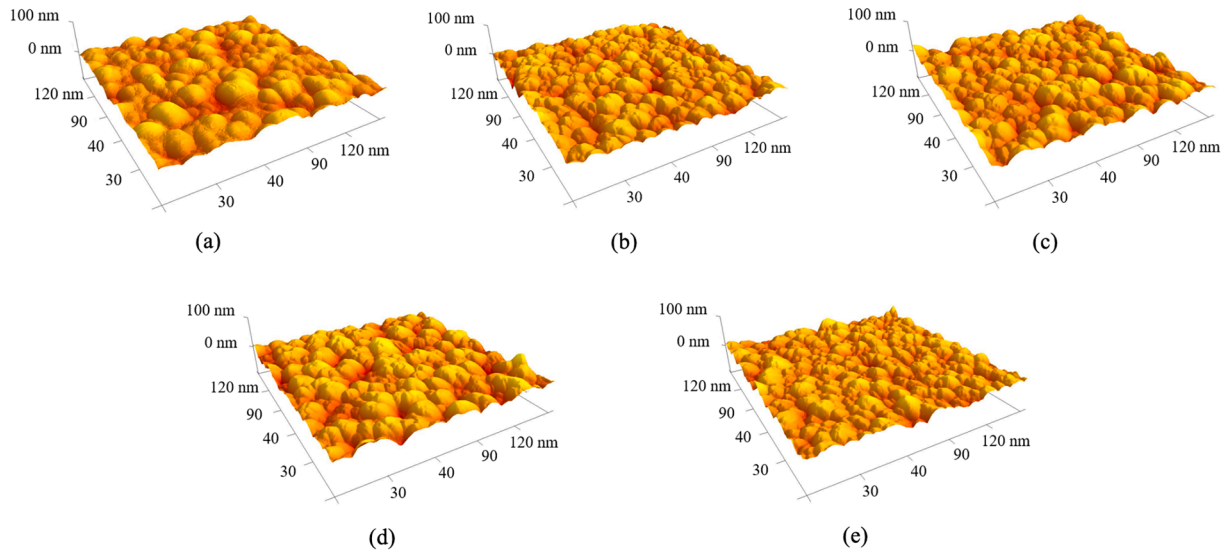

Fig. 5. AFM micrographs show a protruding hemispherical surface morphology as 3D map of the ZnO nanorods as post-annealed at (a) 300 °C, (b) 400 °C, (c) 500 °C, (d) 600 °C and (e) 700 °C, respectively. By mapping the geometrical nano-hemispherical tips from the nanorods diameters of approximately 25 nm can be deduced.

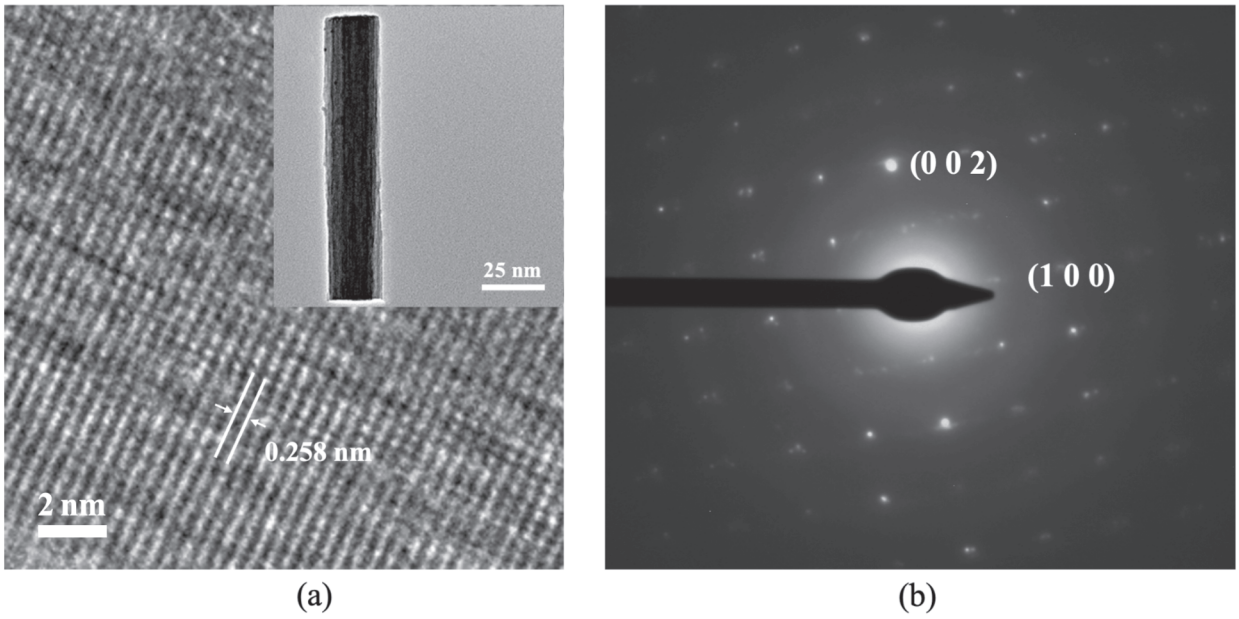

Fig. 6. HRTEM micrographs of (a) an individual ZnO nanorod (in the top right inset) showing atomic interplanar *d*-distance of 0.26 nm and their nanorods as 25 nm diameter. The SAED pattern is shown in (b), and their crystallographic directions of (0 0 2) and (0 0 4) are labelled as per vertical *c*-axis growth.

2p3/2 peaks are independently a Gaussian distribution without shouldering, and thus no peak fitting is required. From the two datasets, it can be concluded that the ZnO contains Zn that is bonded to O in the lattice, while surface defects from oxygen appear to emerge as a post-annealing process is extended to grow the nanorods.

From the UPS analysis, the Au deposited metal and the ZnO nanorods which are post-annealed between 300 °C and 700 °C are studied in Fig. 9. They show the UPS binding energy spectrographs for the Au metal contact and post-annealed ZnO nanorods at their respective temperatures. Based on such optical properties, the UPS data allows the extraction of parameters such as the Fermi edge, valence band maximum (VBM) and cut-off for the nanorods, which can be used to derive an effective band-structure for evaluating Schottky barrier heights for nanostructured based Schottky diode interfaces. Fig. 10 shows the measurement bandgap energies as obtained by optical analysis from the ZnO nanorods post-annealed at (a) 300 °C, (b) 400 °C, (c) 500 °C, (d) 600 °C and (e) 700 °C, respectively. The results for bandgap energies obtained are only used for the band structures modelling.

3.3. Electrical characterisation

To validate the above results five devices are fabricated via semiconductor processing and their electrical properties are analysed by an ultrafine Au based electromechanical spring-loaded probe (1 μm tip diameter) to capture *I-V* data. Data acquisition is obtained via a Keithley 2602B source-meter (down to pA resolutions) between −1.5 V to 1.5 V and 25 to 200 °C voltage biasing and temperature ranges, respectively.

Fig. 11 shows the measured *I-V* data from five Au-ZnO nanorod based Schottky diodes under post-annealing conditions of (a) 300 °C, (b) 400 °C, (c) 500 °C, (d) 600 °C and (e) 700 °C, respectively. In particular,

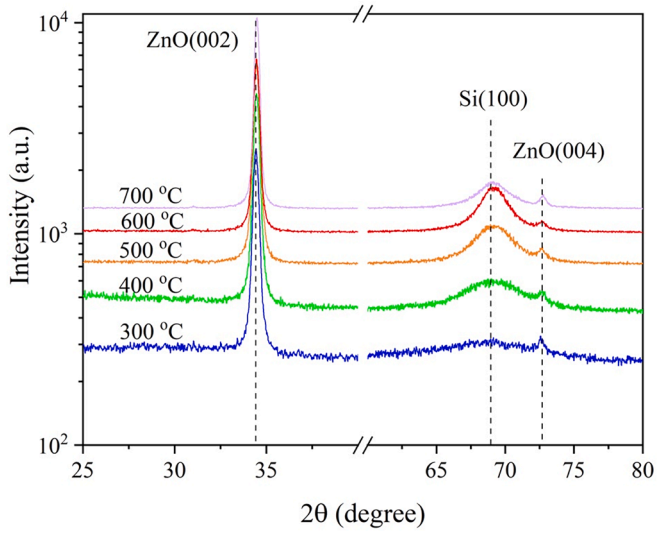

Fig. 7. XRD diffractogram of the ZnO nanorods measured between 25° to 75° 2θ with (0 0 2) and (0 0 4) peaks at 34.3° and 72.8°, indicating nanorod growth in the vertical *c*-axis direction. A broad silicon peak can be observed at 68.2°, indicating the underlying silicon (1 0 0) substrate.

the data between 25 and 200 °C, showing current leakage and rectifying features under forward (FWD rectifying) and reverse (REV current leakage) bias, respectively. Within the forward region of the *I-V* data, OFF and ON regions have been indicated by analysis between nA and μA regions as above specified for nanostructured sensory materials such as nanorod based devices. Specifically, the boundary conditions for Region I is identified as the OFF region, where FE transport takes places, while Region III is identified as the fully saturated ON region where TE transport takes place. Since charging effects have been seen in the cases of nanostructured surfaces, the optimal condition defined to measure sensory materials for their change is considered in Region II, where the balance of charge and temperature energy is equivalent to the Schottky barrier energy and where TFE transport takes place [16].

4. Results

4.1. Material analysis

Analysis of the SEM and AFM material characterisation data shows growth of hemispherical tip ZnO nanorods with a narrow diameter with a long *c*-axis vertical surface morphology for all post-annealed surfaces. In particular, the single crystal based ZnO nanorods distinctively provides minimal bulk defects (verified by TEM and XRD) within the nanorods and therefore focus on a large elongated surface along the side of the nanorods, which serves as the primary current pathway and the surface area for gas adsorption. This also indicates that the majority of defects are surface based and that nanorod formation during growth is highly singular crystal oriented in the vertical direction.

Stoichiometric analysis by XPS shows similar profiles of stoichiometric ZnO for the five nanorod surfaces which the oxygen vacancies (as indicated by the peaks representing the O^{x-} and Zn-O bonds) increase as annealing temperature increases. The data further indicates that ZnO nanorods prepared under 300 °C post-annealing facilitate the least amount of surface defects, as indicated by shouldered peak fit in O1s data as presence of Zn bonds in the lattice is retained in the Zn2p data under post-annealing during nanorod formation. Surface defects will dictate the degree to which the ZnO nanorod Schottky barrier is formed with Au as band bending would occur, reaching charge equilibrium at different energies. Subsequent modelling via simulation using the multi-dielectric energy band diagram program would take into account these changes (in terms of two parameters band gap and electron affinity), which can be both extracted from the UPS data [29].

Energy band diagrams of Au-ZnO nanorods under five post-annealed conditions are modelled. Using the Fermi edge, VBM and cut-off energies from the UPS data, values for E_C, E_F and E_V can be deduced from ZnO nanorods. The positioning of these three energy values is highly crucial as band bending would essentially occur during interface formation with Au to form the Schottky barrier and therefore, can effectively provide an estimated value of the Schottky barrier height.

Fig. 12 shows the energy band diagram of each of the five ZnO nanorod band structures. As indicated in each figure, the position of the ZnO nanorod work function is evaluated located between −4.11 to −4.42 eV, while the work function for Au is deduced to be 5.2 eV. These E_F values reflect the corresponding value for the Fermi level prior to interface formation. While the values for the E_C and E_V energies are positioned between −3.96 to −4.31 eV and −7.03 to −7.38 eV,

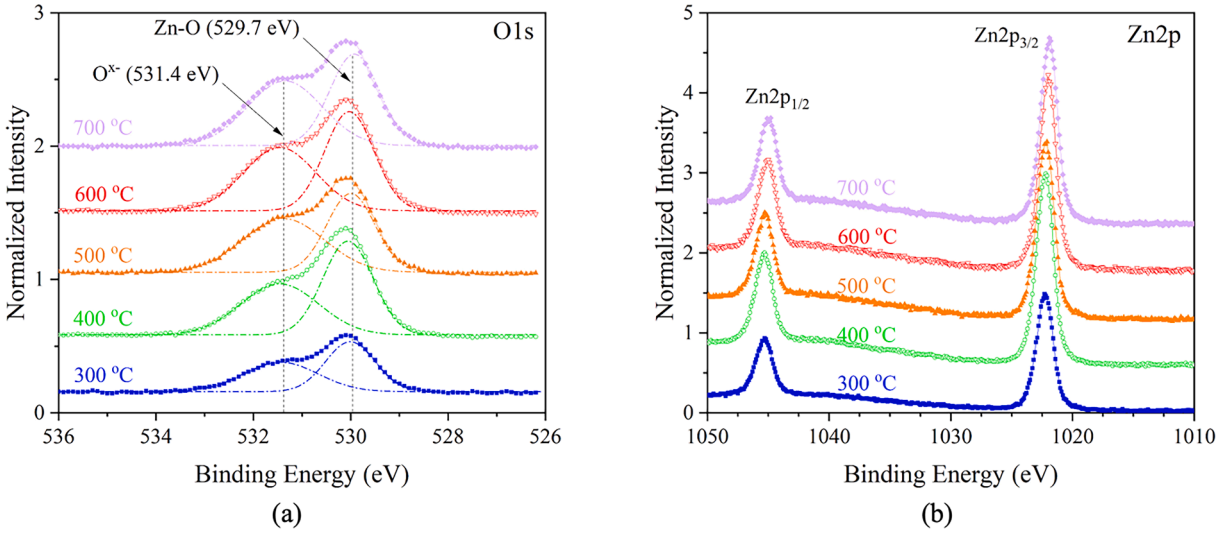

Fig. 8. XPS spectrograph of the binding energies for (a) O1s and (b) Zn2p peaks for the post-annealed ZnO nanorods between temperatures of 300 to 700 °C, respectively. The binding energy peak data are fitted with two subpeaks via Gaussian distributions to discern O^{x-} and Zn-O bonding as provided by the shoulder and head peaks in the O1s data. XPS results indicate a gradual increase in the emergence of surface defects as increasing annealing temperatures are applied.

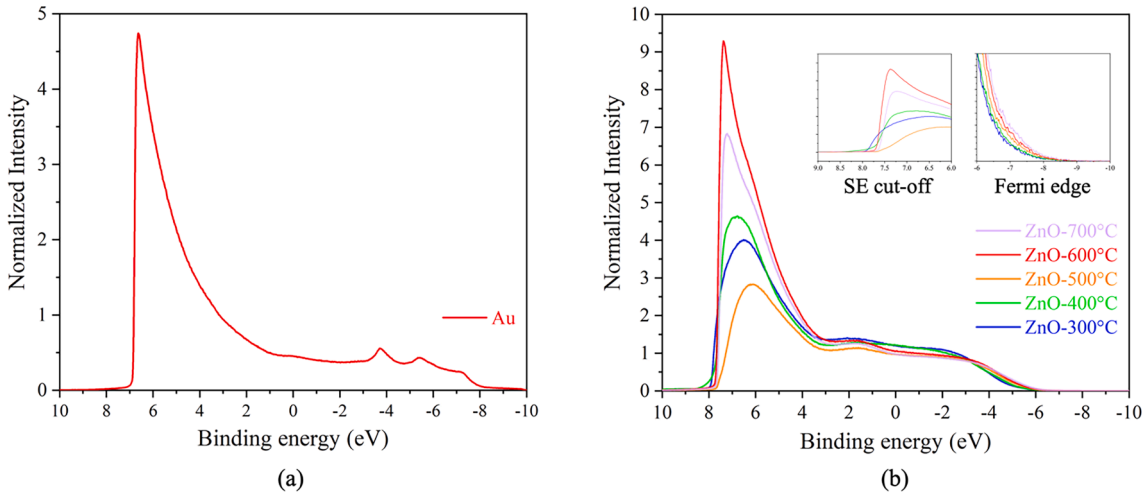

Fig. 9. UPS spectrograph of the binding energy peaks for (a) Au and (b) ZnO nanorods post-annealed between temperatures of 300 to 700 °C, respectively. The figure insets show where the binding energy peak data are linearly extrapolated at the Fermi edge, VBM and cut-off to identify the energy bands for deriving parameter values in ZnO band structure as explained in the results and discussion section.

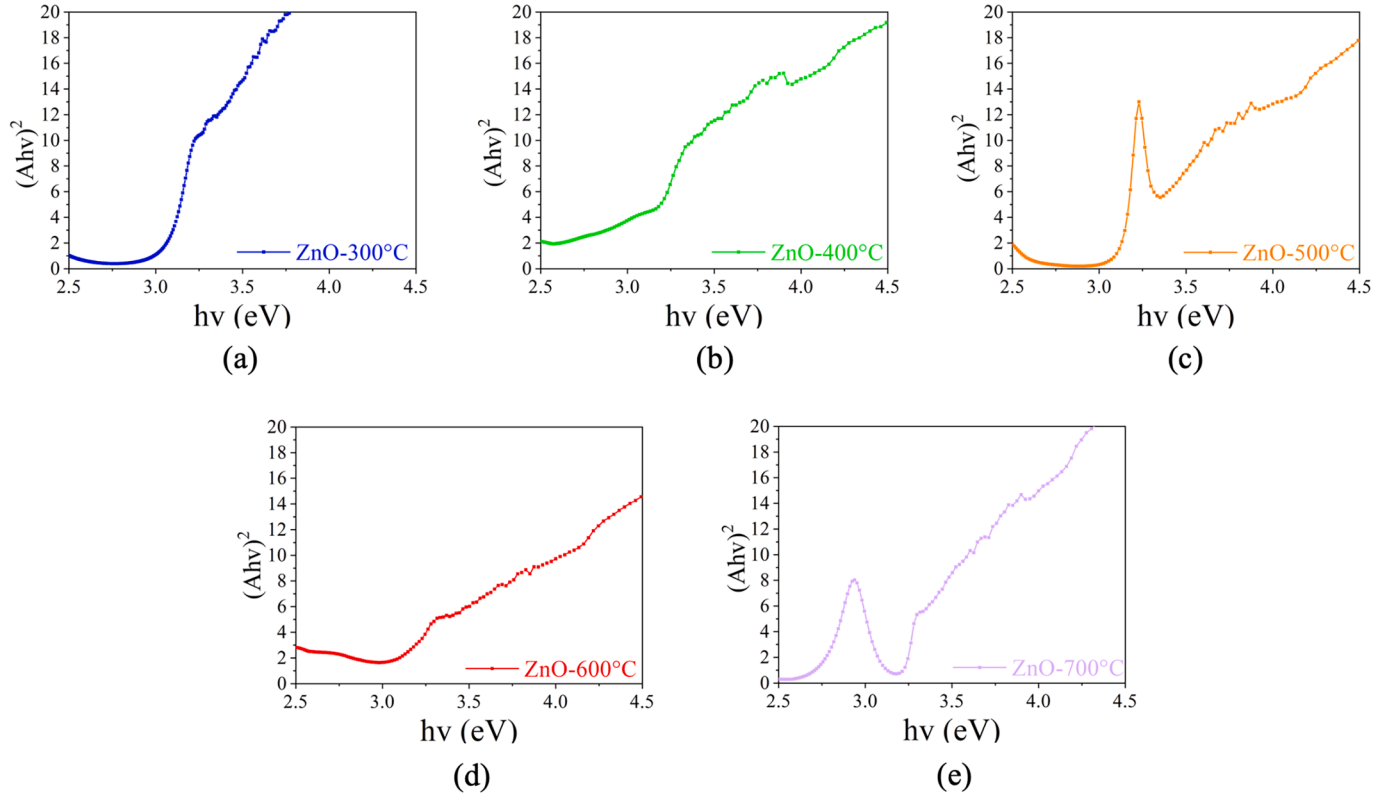

Fig. 10. Tauc plot of the optical absorption data showing the bandgap of ZnO nanorods, which is measured to range from 2.5 eV to 4.5 eV. Bandgap energies can be deduced from nanorods post-annealed at (a) 300 °C, (b) 400 °C, (c) 500 °C, (d) 600 °C and (e) 700 °C are from 3.0 eV to 3.2 eV. Bandgap results are used to deduce the conduction band energy for further band structure modelling.

respectively.

To validate these results, data as obtained by UPS for the bandgap and electron affinity are provided as two input parameters into the multi-dielectric energy band diagram program [31] to simulate each of the five Au-ZnO nanorods cases for intrinsic conditions. No biasing is applied and temperature is provided at 25 °C.

Fig. 13 shows the simulated energy band diagrams for Au-ZnO nanorod band structures as designed by their post-annealing temperatures from 300 to 700 °C. The output of each simulation shows changes in the band bending (slightly noticeable) and energy positions of E_C and E_V gradually, while intrinsic barrier height values appear to be consistent and independent of the two input parameters during band structure formation across all five cases. However, as temperature parameter is increased to 50, 100, 125, 150, 175 and 200 °C (results read from simulator not shown in diagram), the corresponding simulated intrinsic barrier height is decreased to 0.631, 0.608, 0.596, 0.584, 0.571 and 0.559 eV, respectively. These values provided by the simulation serve as approximate boundary conditions for intrinsic Schottky barrier height at zero bias. As bias is applied, the simulator output is unable to provide effective Schottky barrier height values and much less limited to

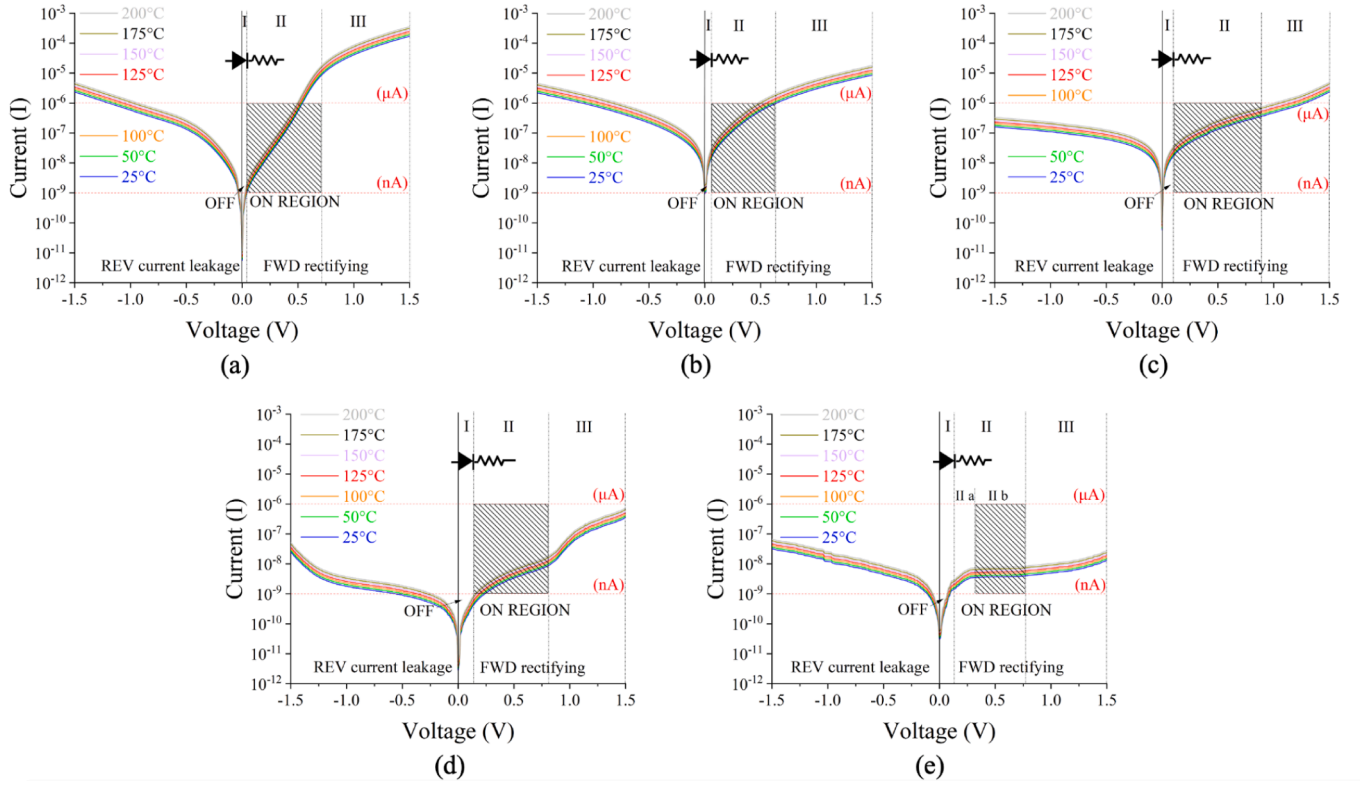

Fig. 11. *I-V* characteristics of Au-ZnO nanorod Schottky diodes as prepared by post-annealing conditions of (a) 300 °C, (b) 400 °C, (c) 500 °C, (d) 600 °C and (e) 700 °C, respectively. Each Au-Pt ZnO nanorod diode is measured under ambient and operational temperatures between 25 and 200 °C. Region II from the *I-V* data (as highlighted) is selected to extrapolate I_0 from Equation (2) via Schottky diode theory and thus estimate a value for each effective nanostructured Schottky barrier height.

intrinsic conditions for planar surface based interfaces. Therefore, an alternative to extract the effective Schottky barrier height values is discussed below.

To locate the optimal position for voltage biasing via TFE for gas sensing requires extracting an effective Schottky barrier height directly from UPS data. To evaluate the Schottky barrier height from band structure as per an energy band diagram, we examine the location of E_C and E_F. During formation of the Schottky barrier, charge flows from the Au metal contact into the semiconductor ZnO nanorod surface to reach charge equilibrium, resulting in band bending alignment. As a result, the Fermi level is shifted to align with the work function of the metal [32]. By postulating the formation of a barrier by finding the difference in the energy positions of ϕ_{Au} and χ_{ZnO} from the UPS data in Fig. 11, values for an effective Schottky barrier height can therefore be deduced artificially via Equation (7) and (8) for the five cases. In theory, using values for ϕ_{UPS} in the five above cases of Au-ZnO nanorods the effective Schottky barrier heights are evaluated as 1.09 eV, 0.91 eV, 0.78 eV, 0.87 eV and 0.81 eV, for the interfaces ZnO-300 °C, ZnO-400 °C, ZnO-500 °C, ZnO-600 °C and ZnO-700 °C, respectively.

4.2. Electrical analysis

Calculation of the effective nanostructure Schottky barrier height for the five Au-ZnO nanorod Schottky diodes is based on TFE theory [16]. To obtain the effective Schottky barrier height via Equation (1) to (5), J is extrapolated for Region II (TFE) from the highlighted section in each *I-V* data. The magnitudes of the ϕ_{IV} values are determined as 1.05, 0.99, 0.81, 0.85, 0.9 eV (at 25 °C). Obtained results are closely comparable and correlated to the intrinsic Schottky barrier height values as output from UPS results. Based on semiconductor theory, Equation (1) represents the Shockley diode equation which values for the Schottky barrier height, and describes the energy position of the band structure elevated under optimal biasing conditions. Therefore, initialising a nanostructured Schottky diode for gas sensory function to detect an external change, a temperature dependent bias can be crucial for the positioning of the Fermi level to maximise the effects of dipolar accumulation and thus, maximise Schottky barrier height modulation. As temperature is increased, recalibration of the biasing is necessary to adapt to the changes in the band structure and therefore analysis of the *I-V* data under different temperatures to calculate the effective Schottky barrier height is required.

Fig. 14 shows the results deduced for the effective Schottky barrier height from *I to V* data (ϕ_{IV}), intrinsic barrier height as modelled from UPS data ϕ_{UPS} and multi-dielectric energy band diagram simulation from the five Au-ZnO nanorods at ambient and elevated temperatures. Results show exponential decrease for ϕ_{IV} in correlation to decreasing operating temperature for ZnO for each of five cases, which shows that values are consistent with ϕ_{UPS} as determined under ambient conditions. Analysis of simulation output showing intrinsic Schottky barrier height indicates linear reduction in Schottky barrier height under temperature dependence under absence of surface defects consideration. Results indicate the importance of UPS analysis, showing how the Schottky barrier height may be modelled to verify the *I-V* analysis for determining Schottky barrier energy for bias positioning to facilitate TFE for gas sensing applications.

In Fig. 14a, effective barrier heights can be observed for the Au-ZnO nanorods located at 1.05, 0.99, 0.81, 0.85, 0.9 eV for annealing temperatures from 300 to 700 °C, respectively. These results are comparable to Fig. 14b as calculated from UPS data while contrasting with results from ideal simulations. The decrease and then increase in values for effective barrier height can be explained by the stoichiometric composition of opposing energy interactions of Zn-O and O^x presence from the XPS data. For example, annealing at 300 to 700 °C provides increasing O^x presence (as indicated by XPS data at 531.4 eV subpeak) as out

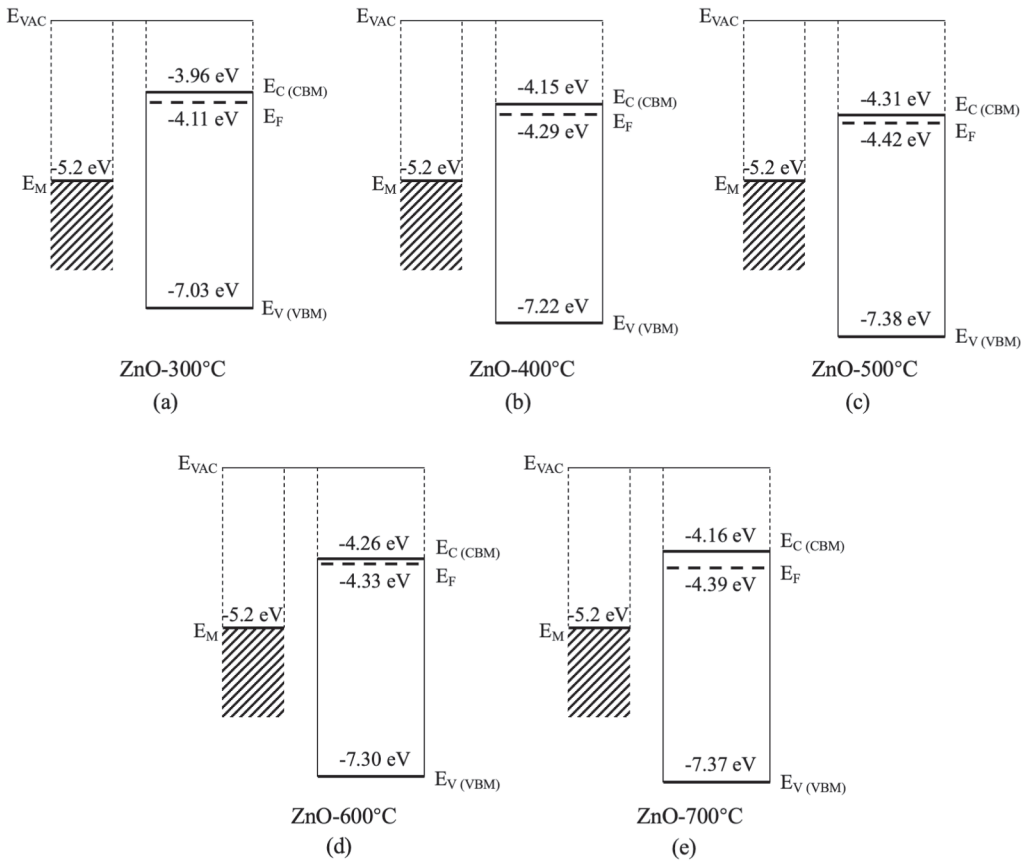

Fig. 12. Energy band diagram of Au and ZnO nanorods ZnO structures as post-annealed at (a) 300 °C, (b) 400 °C, (c) 500 °C, (d) 600 °C and (e) 700 °C are modelled from the UPS data. Positions of the conduction band [22], valence band (E_V) and Fermi level [30] can be deduced from the Fermi edge, VBM and cut-off energies from the UPS data.

diffusion of oxygen in the nanorod lattice under increasing temperatures and 20% oxygen atmosphere. This is counteracted with presence of Zn-O energies at the surface (XPS data at 529.7 eV subpeak) which indicates that Zn diffuses out at temperatures greater than 500 °C. Therefore, the net presence of charge provided by these opposing energies from O^x and Zn-O result in the lowering and raising of effective Schottky barrier height with respect to annealing temperatures.

4.3. Gas sensing analysis

Gas sensing properties of Au-ZnO nanorods in the form of a Schottky diode are examined. Device analysis of dynamic performance via gas response (*I-t*) is measured by gas exposure in a controlled enclosed chamber of 100 sccm volume with input of synthetic air (reference) and H_2 gas (1000 to 10,000 ppm concentration). Sensors are exposed for 5 min exposure time and sufficient time of up to 30 min is allocated for full response recovery by reexposure to synthetic air. Gas response measurements are conducted to observe maximum gas response change at 150 °C, which the optimal operating temperature for ZnO in literature is also reported by findings in [33]. Using results from material and electrical analysis, we have applied the effective Schottky barrier height (from Fig. 14) as the optimum bias voltage to initialise five sets of Au-ZnO nanorods at their corresponding biases, respectively. Measurements are conducted at temperatures of 100 and 150 °C, respectively to simulate dry and optimum conditions.

Gas response based defined by the ratio of currents (measured in air and gas) I_{air}/I_{gas} results from Au-ZnO nanorod Schottky diode (annealed at 500 °C) is considered the highest performing device from Fig. 15. The highest magnitude change of gas response for both tested operating temperatures is also achieved by Au-ZnO nanorods post annealed at 500 °C. Fig. 15**(a)** shows H_2 gas response as measured from each of the five Au-ZnO Schottky diodes as post annealed 300, 400, 500, 600 and 700 °C. This observation is concordant with the findings in the XPS results for ZnO nanorod material formed with the largest presence of surface oxygen defects. The 90% response (τ_R) and recovery (τ_C) time towards H_2 gas for the sensors operating at 100 °C are 4.9 and 20.1 min, respectively. While at 150 °C these times are determined as 4.7 and 16.8 min, respectively. Fig. 15**(b)** shows five gas calibration curves for Au-ZnO Schottky diodes of Fig. 15(a) at 100 °C and 150 °C. As can be seen in the results, each nanostructured Schottky diode responds to H_2 gas with an exponential gas response with respect to gas concentration, especially after the 5000 ppm, which indicates suitability specifically for large storage vessels to contain hydrogen fuel requiring sufficient sensitivity for measuring H_2 concentrations at 5000 ppm (and far above 10,000 ppm) over long periods of time. To develop smarter digital gas storage regulators for on-site or portable gas cylinders and even for future hydrogen powered vehicles, highly sensitive gas sensors that aim to indicate concentrations between 99% down to 0.5% (5000 ppm) would be advantageous for future potential applications in monitoring gaseous refuelling, calibration and redeployment.

Table 1 shows a performance comparison for different based H_2 gas sensors incorporating Au-ZnO nanorods are benchmarked with the literature. Data shows gas performance of Au-ZnO nanorods annealed at 500 °C demonstrate a gas response to H_2 gas at a concentration of 10,000 ppm highly comparable and exceeding fabrication methods as reported by [34,35] while operating at 100 and 150 °C. Results also show that the H_2 gas concentration at the lower threshold of 5,000 ppm detection provides the highest gas response as achieved under optimised

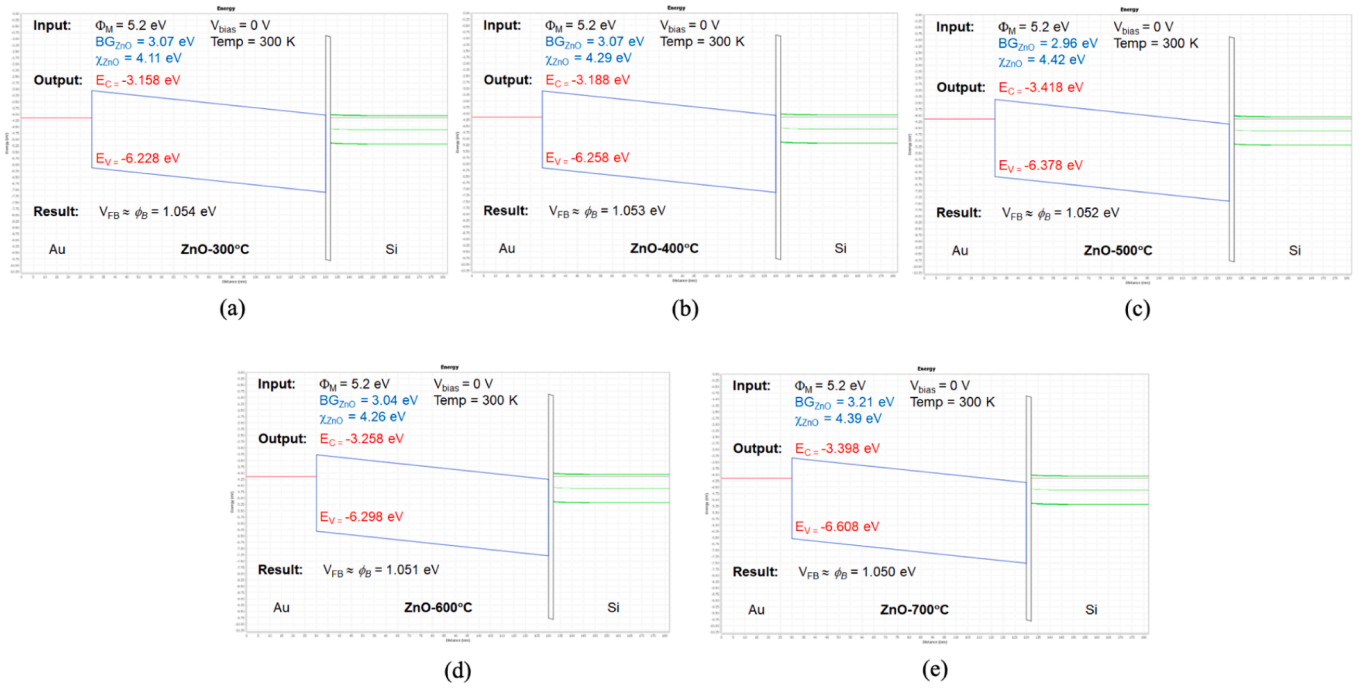

Fig. 13. Energy band diagrams of Au-ZnO band structures for the five cases based on the UPS data using bandgap (BG) and electron affinity to estimate the conditions of the band bending and thus obtain estimates for the Schottky barrier height. The UPS data is based on the five cases of Au-ZnO nanorods as post-annealed at (a) 300 °C, (b) 400 °C, (c) 500 °C, (d) 600 °C and (e) 700 °C are evaluated as 4.11, 4.29, 4.42, 4.33 and 4.39 eV, respectively.

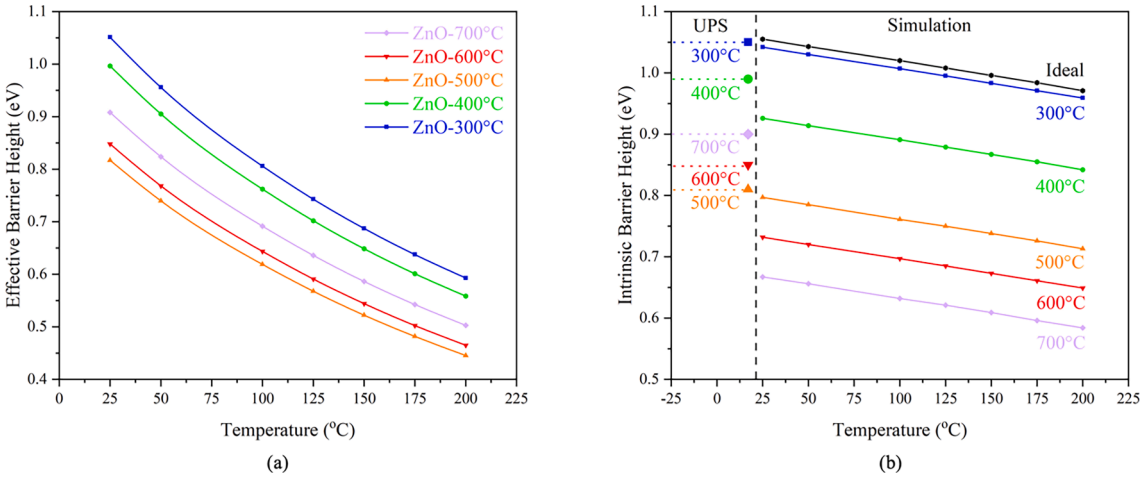

Fig. 14. (a) Effective Schottky barrier heights and (b) Intrinsic barrier heights under operating temperatures between 25 and 200 °C as evaluated from *I to V* data, UPS data and Simulation data from the Au-ZnO nanorods prepared under different annealing temperatures (300 to 700 °C).

conditions.

5. Conclusions

In this work, optimum operating conditions for five Au-ZnO nanorod Schottky diodes are found using an optical (UPS) and electrical (*I-V*) measurement methodology. Our novel approach models the band structure to deduce the Schottky barrier height under thermionic field emission theory and is verified with a multi-dielectric energy band diagram simulation. By finding the relationship between the effective barrier height and operating temperature, the optimum voltage bias can be applied to maximise the performance of the sensor to detect H_2 under a dry condition of 100 and optimum temperature of 150 °C. Gas response results validated the above postulations for Au-ZnO nanorod Schottky diodes, while the highest performing device is ascribed to the nanorod fabrication subsequent to post-annealing ZnO nanorods at 500 °C.

CRediT authorship contribution statement

Kun Cao: Conceptualization, Methodology, Investigation, Writing - original draft. **Guanyi Gong:** Software, Validation. **Xiangyang Guo:** Resources, Visualization. **Yanling He:** Formal analysis, Data curation. **Francis Chi Chung Ling:** Formal analysis, Writing - review & editing. **Wanyin Ge:** Validation. **Alan Man Ching Ng:** Conceptualization, Methodology, Supervision. **Yongxiang Li:** Investigation, Resources, Conceptualization, Supervision, Writing - review & editing. **Jerry Yu:** Methodology, Project administration, Writing - review & editing.

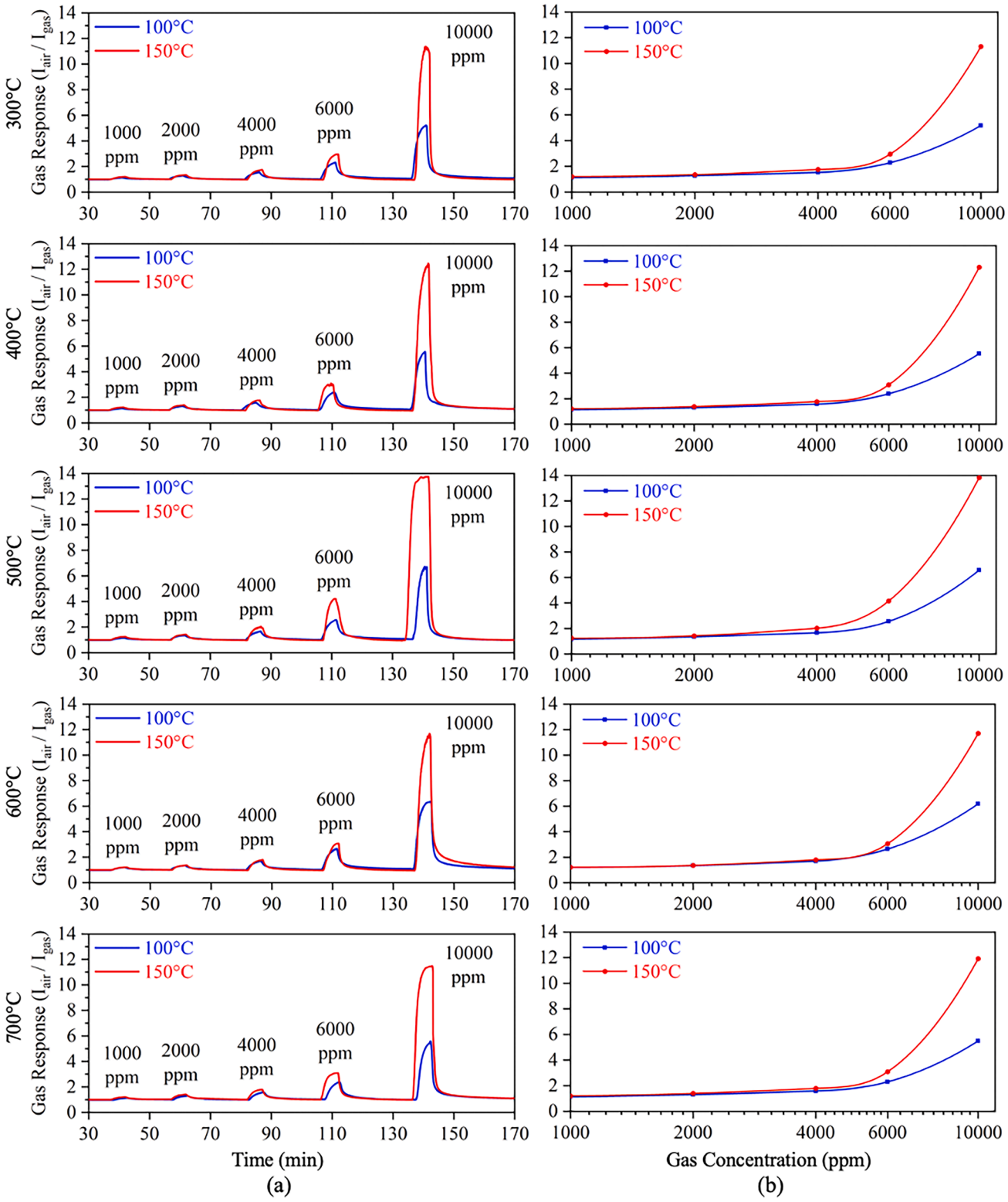

Fig. 15. (a) Gas response (I_{air}/I_{gas}) to H_2 measured from Au-ZnO nanorod Schottky diodes (annealed from 300 to 700 °C) while operating temperatures of 100 and 150 °C as initialised under their optimum operating biases (corresponding to effective Schottky barrier height in Fig. 14). H_2 gas flow is 100 sccm with 5 min exposure time under different gas concentrations between 1000 and 10,000 ppm, sequentially. (b) Gas calibration curve to H_2 showing response magnitude and response time as analysed under 100 °C and 150 °C.

Declaration of Competing Interest

The authors declare the following financial interests/personal relationships which may be considered as potential competing interests: [Yongxiang Li reports financial support was provided by Diagnoses Melbourne Pty Ltd].

Table 1
Comparison benchmark of nanostructured H_2 gas sensors (above 5000 ppm) with similar works in the literature.

Nanostructure type	Fabrication method	Gas concentration (ppm)	Gas Response	Operating temperature (°C)	References
Nanorod	Pulsed Laser Deposition	10 000	13.83	150	This work
Nanorod	Pulsed Laser Deposition	10 000	6.57	100	This work
ZnO nanorods	Chemical Bath Deposition	10 000	5	200	[34]
Nb_2O_5-core/ZnO-shell nanorod	Thermal Oxidation	10 000	4.5	300	[35]
ZnO NPs and rGO-ZnO NPs	Chemical Vapor Deposition	10 000	4	25	[36]
ZnO thin films	PLD	5 000	2.9	300	[37]
Pd-SnO_2/MoS_2	Hydrothermal synthesis	5 000	1.18	25	[38]
Nanorod	Pulsed Laser Deposition	5 000	4.15	150	This work
Nanorod	Pulsed Laser Deposition	5 000	2.56	100	This work

Data availability

No data was used for the research described in the article.

Acknowledgments

This research is supported by the technical resources and expertise from Micro Nano Research Facility (MNRF) in the Victorian Node of the Australian National Fabrication Facility (ANFF), and Microscopy & Microanalysis Facility (RMMF) of RMIT University, in collaboration with University of Hong Kong (Hong Kong) and Southern University of Science and Technology (SUSTech, China). The authors gratefully acknowledge the support of Diagnoses Melbourne Pty Ltd for their generous financial contribution to this research project.

References

[1] A. Dey, Semiconductor metal oxide gas sensors: A review, Mater. Sci. Eng. B 229 (2018) 206–217.
[2] Y. Luo, C. Zhang, B. Zheng, X. Geng, M. Debliquy, Hydrogen sensors based on noble metal doped metal-oxide semiconductor: A review, Int. J. Hydrogen Energy 42 (2017) 20386–20397.
[3] G. Fiori, F. Bonaccorso, G. Iannaccone, T. Palacios, D. Neumaier, A. Seabaugh, S. K. Banerjee, L. Colombo, Electronics based on two-dimensional materials, Nat. Nanotechnol. 9 (2014) 768–779.
[4] S. Das, V. Jayaraman, SnO_2: A comprehensive review on structures and gas sensors, Prog. Mater Sci. 66 (2014) 112–255.
[5] V. Galstyan, E. Comini, C. Baratto, G. Faglia, G. Sberveglieri, Nanostructured ZnO chemical gas sensors, Ceram. Int. 41 (2015) 14239–14244.
[6] J. Zhang, X. Liu, G. Neri, N. Pinna, Nanostructured materials for room-temperature gas sensors, Adv. Mater. 28 (2016) 795–831.
[7] Y. Liu, J. Yu, W.M. Tang, P. Lai, On the voltage dependence of sensitivity for Schottky-type gas sensor, Appl. Phys. Lett. 105 (2014) 223503.
[8] M.-W. Ahn, K.-S. Park, J.-H. Heo, J.-G. Park, D.-W. Kim, K.J. Choi, J.-H. Lee, S.-H. Hong, Gas sensing properties of defect-controlled ZnO-nanowire gas sensor, Appl. Phys. Lett. 93 (2008) 263103.
[9] X. Zhou, A. Wang, Y. Wang, L. Bian, Z. Yang, Y. Bian, Y. Gong, X. Wu, N. Han, Y. Chen, Crystal-defect-dependent gas-sensing mechanism of the single ZnO nanowire sensors, ACS Sensors 3 (2018) 2385–2393.
[10] M. Al-Hashem, S. Akbar, P. Morris, Role of oxygen vacancies in nanostructured metal-oxide gas sensors: A review, Sens. Actuators B 301 (2019) 126845.
[11] A. Yu, J. Qian, H. Pan, Y. Cui, M. Xu, L. Tu, Q. Chai, X. Zhou, Micro-lotus constructed by Fe-doped ZnO hierarchically porous nanosheets: preparation, characterization and gas sensing property, Sens. Actuators B 158 (2011) 9–16.
[12] X. Wang, W. Liu, C. Wang, S. Zhang, M. Ding, X. Xu, Enhanced formaldehyde gas sensing performance of ternary $CuBi_2O_4$ oxides through oxygen vacancy manipulation and surface platinum decoration, Sens. Actuators B 344 (2021) 130190.
[13] C. Buono, D. Mirabella, P. Desimone, C. Aldao, Effects of Schottky barrier height fluctuations on conductivity: Consequences on power-law response in tin oxide gas sensors, Solid State Ion. 369 (2021) 115725.
[14] Y. Kim, S.-K. Kang, N.-C. Oh, H.-D. Lee, S.-M. Lee, J. Park, H. Kim, Improved sensitivity in schottky contacted two-dimensional MoS_2 gas sensor, ACS Appl. Mater. Interfaces 11 (2019) 38902–38909.
[15] M. Kumar, V.S. Bhati, M. Kumar, Effect of Schottky barrier height on hydrogen gas sensitivity of metal/TiO_2 nanoplates, International Journal of Hydrogen Energy 42 (2017) 22082–22089.
[16] S.M. Sze, Y. Li, K.K. Ng, Physics of semiconductor devices, John Wiley & Sons, 2021.
[17] C.J. Delerue, M. Lannoo, Nanostructures: Theory and modeling, Springer Science & Business Media, 2013.
[18] M. Montero-Muñoz, J. Ramos-Ibarra, J.E. Rodríguez-Páez, M.D. Teodoro, G. E. Marques, A.R. Sanabria, P.C. Cajas, C.A. Páez, B. Heinrichs, J.A. Coaquira, Role of defects on the enhancement of the photocatalytic response of ZnO nanostructures, Appl. Surf. Sci. 448 (2018) 646–654.
[19] L. Schmidt-Mende, J.L. MacManus-Driscoll, ZnO–nanostructures, defects, and devices, Mater. Today 10 (2007) 40–48.
[20] R.A. Wahyuono, F. Hermann-Westendorf, A. Dellith, C. Schmidt, J. Dellith, J. Plentz, M. Schulz, M. Presselt, M. Seyring, M. Rettenmeyer, Effect of annealing on the sub-bandgap, defects and trapping states of ZnO nanostructures, Chem. Phys. 483 (2017) 112–121.
[21] K. Ejderha, A. Turut, Dependence of electrical properties of Ni/n-GaP/Al Schottky contacts on measurement temperature and thermal annealing, J. Electron. Mater. 50 (2021) 6741–6747.
[22] A. Turut, On current-voltage and capacitance-voltage characteristics of metal-semiconductor contacts, Turk. J. Phys. 44 (2020) 302–347.
[23] N. Gong, T.-P. Ma, A study of endurance issues in HfO_2-based ferroelectric field effect transistors: Charge trapping and trap generation, IEEE Electron Device Lett. 39 (2017) 15–18.
[24] K.W. Cheung, J. Yu, D. Ho, Determination of the optimal sensing temperature in Pt/Ta_2O_5/MoO_3 Schottky contacted nanobelt straddling heterojunction, Sensors 18 (2018) 3770.
[25] J.H.D. Eland, Photoelectron spectroscopy: An introduction to ultraviolet photoelectron spectroscopy in the gas phase, Elsevier, 2013.
[26] T.M. Pan, T.F. Lei, T.S. Chao, M.C. Liaw, F.H. Ko, C.P. Lu, One-step cleaning solution to replace the conventional RCA two-step cleaning recipe for pregate oxide cleaning, J. Electrochem. Soc. 148 (2001) G315.
[27] C. Kun, Y. He, Y. Li, A. Ng, J. Yu, A room temperature hydrocarbon electronic nose gas sensor based on schottky and heterojunction diode structures, IEEE Electron Device Lett. 41 (2019) 163–166.
[28] A. El Haimeur, A. Slassi, A. Pershin, D. Cornil, M. Makha, E. Blanco, M. Dominguez, H. Bakkali, Reducing p-type Schottky contact barrier in metal/ZnO heterostructure through Ni-doping, Appl. Surf. Sci. 545 (2021) 149023.
[29] S. Hüfner, Photoelectron spectroscopy: Principles and applications, Springer Science & Business Media, 2013.
[30] V.V. Krivetskiy, M.D. Andreev, A.O. Efitorov, A.M. Gaskov, Statistical shape analysis pre-processing of temperature modulated metal oxide gas sensor response for machine learning improved selectivity of gases detection in real atmospheric conditions, Sens. Actuators B 329 (2021) 129187.
[31] N.A. Gayala, C.R.A.J. Chelliah, Simulation and comparison of capacitance voltage characteristics due to the effect of varying temperatures for MOS quantum dot device configurations in Al/Pbse/ZnO/Si and Al/Pbte/ZnO/Si, in: AIP Conference Proceedings, AIP Publishing, 2023.
[32] R.T. Tung, The physics and chemistry of the Schottky barrier height, Appl. Phys. Rev. 1 (2014) 011304.
[33] P. Bhat, SK. Naveen Kumar, P. Nagaraju, Fabrication of ultrasensitive hexagonal disc structured ZnO thin film sensor to trace nitric oxide, J. Asian Ceram. Soc. 9 (2021) 96–105.
[34] N. Banerjee, S. Roy, C. Sarkar, P. Bhattacharyya, Pd modified ZnO nanorod based high dynamic range hydrogen sensor, in: In: 2013 13th IEEE International Conference on Nanotechnology (IEEE-NANO 2013), 2013, pp. 682–685.
[35] S. Park, S. Park, S. Lee, H.W. Kim, C. Lee, Hydrogen sensing properties of multiple networked Nb_2O_5/ZnO core–shell nanorod sensors, Sens. Actuators B 202 (2014) 840–845.
[36] S. Das, S. Roy, T.S. Bhattacharya, C.K. Sarkar, Efficient room temperature hydrogen gas sensor using ZnO nanoparticles-reduced graphene oxide nanohybrid, IEEE Sens. J. 21 (2020) 1264–1272.
[37] Y. Liu, T. Hang, Y. Xie, Z. Bao, J. Song, H. Zhang, E. Xie, Effect of Mg doping on the hydrogen-sensing characteristics of ZnO thin films, Sens. Actuators B 160 (2011) 266–270.
[38] D. Zhang, C. Jiang, Y. Zhang, Room temperature hydrogen gas sensor based on palladium decorated tin oxide/molybdenum disulfide ternary hybrid via hydrothermal route, Sens. Actuators B 242 (2017) 15–24.

Kun Cao is an experienced Electronics Engineer undertaking PhD candidature in developing Breath Analyser based Nanosensor Components and Systems at RMIT University with scientific journal publication and patent in Olfactory Sensing Technology. Strong experience in R&D technology development and management focusing on 2D materials, Gas sensor array, embedded hardware development, electronics circuit design and AI algorithm.

Guanyi Gong received his M.Eng. degree in Electronic Engineering from RMIT University, Australia in 2021. Currently, he is pursuing a research master's degree under the supervision of Prof. Yongxiang Li. His research study is the fabrication of piezoelectric material devices based on 3D printing, including piezoelectric ceramics, piezoelectric polymers I and piezoelectric composites.

Xiangyang Guo received his MEng degree from the School of Electrical and Electronic Engineering at RMIT University in 2019. He is currently a PhD student in Electronic and Telecommunications Engineering at the School of Engineering, RMIT University, under the supervision of Prof. Yongxiang Li. His research topic focuses on 2D SnX (S, Se) material films by liquid-metal exfoliation and their applications for piezoelectric and gas sensing devices.

Yanlin He received her M.S. degree from the Chinese University of Hong Kong.

Now she is expected to finish her Ph.D. study at the department of physics, the University of Hong Kong. Her research mainly focusses on the design and synthesis of nanostructure materials, surface properties characterization and catalysis.

Francis Chi Chung Ling is an associate professor of the Department of Physics in The University of Hong Kong. He obtained his PhD from The University of Hong Kong. He was elected as a Fellow of IOP, UK in 2006. Francis' research interest is in defect characterization and control in semiconductor materials with focus in the applications in optoelectronic and high power devices.

Wanyin Ge, professor. He graduated from Shanghai Institute of Ceramics, Chinese Academy of Sciences in 2005. In 2009, he received his PhD degree from Kyoto Institute of Technology (Japan). From 2009–2016, he served successively as a postdoctoral GCOE (Global Chief of Executive) in Kyushu University, Kyoto University, Japan, and a research fellow in the University Of Oklahoma, USA. In 2008, he was awarded the National Scholarship for Excellent Self-funded Overseas Students by the Ministry of Education of China. In 2016, he returned to China and worked as a team leader of two-dimensional functional materials and sensor group.

Alan Man Ching Ng had been an Associate Professor in the Department of Physics in Southern University of Science and Technology (SUSTech) since 2011. He became the Associate Director of the Core Research Facilities of SUSTech since 2019. His research has been focused on binary metal oxide materials, mainly on their nanostructures fabrication, surface properties characterization, optoelectronic device applications, heterogeneous photocatalysis, energy and environmental applications. He has published more than 120 journal articles and conference proceedings with over 5000 citations and h-index 32.

Yongxiang Li is a professor in the Electronic & Telecommunications Discipline, School of Engineering, RMIT University. His research interests are electronic materials and devices, focusing on electroceramics, sensors and actuators, LTCC technique and ceramic microsystems. He has committed to several professional committees and memberships, including Asian Ferroelectric Association (AFA), IEEE Senior Member, American Ceramic Society, Material Research Society, and Materials Australia.

Jerry Yu has 15 years reputation in Applied Research and Development with 4 highly successful MVPs trading and earning over HK$7.3M in project revenue to date. Dr. Yu has been awarded over HK$ 1.6M in Industry Contracts and Academic Research Funding with 49 Scientific Publications and two Patents. Dr. Yu served Ten years in academia at HKU, CityU and PolyU (HK) in research on fundamental sensory technology and developing applied industry solutions in China and the Asia-Pacific. Dr. Yu holds 2 honorary research fellow positions at SUSTec University (Shenzhen, China) and RMIT University (Melbourne, Australia) and is the sole 2012 RMIT Vice-Chancellor's Doctoral Research Excellence Award recipient and the 2010 Cheung Kong Research Fellowship Endeavour Australia recipient. Dr. Yu's expertise in semiconductor nanofabrication, Quantum electronic nose devices and low power electronics, gas nanosensors and new applied materials.